GMR
The Original

REMOVAL OF PB(II), HG(II), CR(VI), AND NI(II) FROM WASTEWATER VIA COMPLEXATION-ASSISTED ADSORPTION ONTO MESOPOROUS ADSORBENT: EFFECTS OF PH, TEMPERATURE, AND PORE STRUCTURE

Veeresh Halemane[1*], Dr. Vijaya Kumar Durg[2]

[1*]Department of Chemistry, SSAS Government First Grade College, Hosapete-583201 (Karnataka), India. veereshhalemanechem@gmail.com;
[2]Department of Chemistry, Bhemanna Khandre Institute of Technology – Bhalki-585413 (Karnataka), Inida.
*Corresponding Author: Email: veereshhalemanechem@gmail.com

ABSTRACT

Eluting the toxic heavy metals in wastewater is also a highly important environmental challenge because they are persistent and bioaccumulative as well as have detrimental health impacts. A functionalized mesoporous adsorbent was prepared in this research through amine grafting on a mesoporous silica structure and tested in adsorbing Pb(II), Hg(II), Cr(VI), and Ni(II) on aqueous solutions using complexation-based adsorption. Successful functionalization and maintenance of the mesoporosity of the structure was confirmed by structural characterization with the BET surface area of 412 $m^2 g^{-1}$ a high surface area and an average pore diameter of 6.7 nm. Experiments involving batch adsorption were carried out under different conditions of pH (2-10), temperature (20-60ºC) and metal concentration (10-200 mg L^{-1}) in order to ascertain the conditions of optimal behavior and adsorption.

The removal was also very dependent on solution pH and metal speciation with the best results being a pH of 5 with Pb(II) and Hg(II), pH of 6 with Ni(II), and pH of 3 with Cr(VI). The temperature raised the adsorption capacity and this is a sign of an endothermic process. Langmuir and Freundlich models provided a good characterization of the equilibrium data, implying that the adsorption took place on homogeneous adsorbing amine sites with a small portion of heterogeneity. The maximum adsorption capacities were 182.4, 165.7, 138.6 and 121.3 mg g^{-1} of Pb(II), Hg(II), Cr(VI), and Ni(II), respectively. Spontaneous chemisorption was proved by means of thermodynamic parameters ($\Delta H° = 19\text{-}28$ kJ mol^{-1}; $\Delta G° < 0$).

Enhanced adsorption behavior is probably explained by the synergistic activity of mesoporous diffus[]ion channels, large surface area, and an effective coordination interaction between amine functionalities and metal ions. The results indicate that the functionalized mesoporous adsorbents are valuable materials to be utilized effectively and selectively in the removal of various heavy metals in wastewater and justify their possible use in modern installations of water purification.

KEYWORDS: Heavy metal removal; Mesoporous adsorbent; Complexation-assisted adsorption; Pb(II); Hg(II); Cr(VI); Ni(II)

INTRODUCTION

The high rate of industrialization, mining, electroplating, battery production, tanning, and metallurgy have caused massive inflow of heavy-metal-containing effluents into the water. Lead (Pb), mercury (Hg), chromium (Cr), and nickel (Ni) are toxic metals that are not biodegradable and accumulate in the biological systems with high levels of severity to bioaccumulation and biomagnification risks to the ecosystems and human health (Jadoun et al., 2023; Garcia-Avila et al., 2025). Such metals can forever remain in the water, and sediments where they contaminate drinking-water supply sources and farmland soils resulting in neurological, renal, and cancer-causing impacts even at low levels (Garcia-Avila et al., 2025). Therefore, it has been indicated that regulatory authorities across the world have set strong discharge limits of heavy metals in wastewater, and efficient and sustainable technologies are required to remove them.

The traditional methods of treatment of heavy-metals in wastewater are chemical precipitation, ion exchange, membrane filtration, electrochemical treatment and coagulation-flocculation. Nevertheless, these methods usually have some weaknesses in that they are costly to operate, produce toxic sludge, fail to eliminate at low concentration, and their treatment demands are intricate (Qasem et al., 2021). During the last few years, adsorption has become one of the most promising methods of heavy-metal remediation due to its simplicity, relatively low costs, flexibility of its application, and the capability to extract metals at trace levels without any secondary pollutant production (Kumar et al., 2024; Ayach et al., 2024). The process of Adsorption entails a deposition of the metal ions on the body or inside the tube of these solid adsorbents in the form of physical interactions or electrostatic bonding, ion exchange, and chemical bonds involving functional groups (Yousef et al., 2024).

The physicochemical characteristics of adsorbent and in particular the surface area, the size distribution of pores, and surface functionalization determine the performance of adsorption systems. Hydrated metal ions can diffuse more easily into internal adsorption spaces because highly porous mesopores materials allow easier access to active sites and

immediate diffusion into the internal cavities of the material, thus increasing the adsorption capacity (Yousef et al., 2024). Hydroxyl, carboxyl, amine and thiol functional groups can coordinate metals, which leads to chemisorption and selectivity. The recent reports indicated that surface-modified carbons, polymers, clays, and nanocomposites have a much better pre-adsorption capacity compared to unmodified ones, as they are characterized by a more sophisticated pore framework and extensivity of the complexation sites (Jadoun et al., 2023; Kumar et al., 2024).

Solution pH and temperature are the two operational parameters that are believed to be the most significant parameters governing adsorption behavior. The pH of the solution transforms surface charge of the adsorbent, as well as speciation of metal ions, and, as a consequence, influences electrostatic attraction and complexation responses. The majority of heavy-metal adsorption experiments show the best performance in alkaline (pH 3-9), in which the competition with protons is reduced to the minimum, and the metal hydrolysis is weakened (Garcia-Avila et al., 2025). Temperature impacts adsorption kinetics and thermodynamics and gives an understanding of whether an adsorption process is endothermic or exothermic and whether the process is physisorption or chemisorption (Youssif et al., 2024). These parameters are therefore important and should be systematically analyzed in the development of effective treatment systems.

Isotherm models; common models used to describe adsorption equilibrium include the Langmuir and Freundlich models that give a quantitative data on the capacity of adsorbing, the surface heterogeneity, and affinity of adsorbate and adsorbent. Good consensus of the data obtained through the use of these models with heavy-metal adsorption has been reported through numerous studies particularly in recent times, supporting the adsorption process via monolayer or heterogeneous adsorption processes based on the adsorbs structure (Srinivasan, 2025). However, one of the greatest challenges that have been found in the literature is the concomitant deposition of various metal ions under different environmental conditions and the mechanistic connection between the pore structure and complexation-assisted adsorption (Qasem et al., 2021).

Thus, it is clear that the systematic empirical studies, which would combine pore-size characterization with multi-metal adsorption behavior under a variety of pH and temperature regimes, are still needed. These studies are necessary to understand the adsorption mechanisms, optimize the working conditions and come up with high performance adsorbents to be used in the practical application to real wastewater treatment. This gap is fulfilled in the current study where removal of Pb(II), Hg(II), Cr(VI), and Ni(II) in aqueous solutions with the use of a mesoporous adsorbent is considered, with pore structure, complexation interaction, and adsorption isotherm modeling being the focus.

2. MATERIALS AND METHODS

2.1 Materials

The chemicals that were used were all of analytical grade and were not purified any further. $(Pb(NO_3)_2)$, $HgCl_2$, $K_2Cr_2O_7$, and $NiSO_4 \cdot 6H_2O$ were used as a source of Pb(II), Hg(II), Cr(VI), and Ni(II), respectively. pH adjustment was done by the use of nitric acid (HNO_3) and sodium hydroxide (NaOH). All preparations were done using deionized water (18.2 MΩ·cm).

To high surface area and coordination sites to complex with heavy-metal ions a mesoporous silica support, which contained amine groups, was synthesized.

Table 1. Chemicals and materials used in the study

Chemical / Material	Formula	Purity (%)	Supplier	Use
Lead nitrate	$Pb(NO_3)_2$	≥99	Merck	Pb(II) source
Mercuric chloride	$HgCl_2$	≥99	Sigma-Aldrich	Hg(II) source
Potassium dichromate	$K_2Cr_2O_7$	≥99	Merck	Cr(VI) source
Nickel sulfate hexahydrate	$NiSO_4 \cdot 6H_2O$	≥98	SRL	Ni(II) source
Nitric acid	HNO_3	65	Merck	pH adjustment
Sodium hydroxide	NaOH	≥98	Merck	pH adjustment
Mesoporous silica	SiO_2	—	Sigma-Aldrich	Adsorbent support
Amine ligand	—	≥98	TCI	Functionalization

2.2 Generation of Functionalized Mesoporous Adsorbent

To eliminate physisorbed Water In Mesoporous silica, it was thermally treated at 120ºC over a period of 4 h. To increase silanol reactivity, it was heated at 120ºC. Silica (5 g), a given quantity of the substance was treated with anhydrous toluene (100 mL) and ultrasonic mixing of the mixture took place (30 min). A dropwise addition of an amine-based ligand (10 wt % with respect to silica) was carried out under nitrogen atmosphere and refluxing the suspension 110ºC 12h lagged covalent grafting of the silica surface.

This product was filtered, dried the product using ethanol and deionized water in order to eliminate unreacted species and dried the product at the 80ºC temperature within the 24 h period. The dry fine material was burnt to a fine state of 100-200 um particle size after which it was sieved and stored under a desiccator.

2.3 Adsorbent Characterization

2.3.1 Surface Morphology

SEM was utilized to study the morphology of particles, roughness on the surface and pore structure.

2.3.2 Distribution of Surface Area and Pores

The adsorption, desorption isotherms of nitrogen were recorded at 77 K upon a de-gasification of the samples at 120ºC during 6 h. The Brunauer-Emmett-Teller (BET) technique was used to determine the specific surface area, and the Barrett-Joyner-Halenda (BJH) model was used to determine pore size distribution.

2.3.3 Functional Groups

The grafting of amines was confirmed in the Fourier transform infrared (FTIR) spectra (4000-400 cm^{-1}) and the functional groups active in adsorption.

2.3.4 Point of Zero Charge (pHpzc)

Surface charge behavior was determined by the pH drift method. Adsorbent (0.05 g) was incubated with 0.01M NaCl solutions of initial 2-11 pH over the 24 h period. The pHpzc was a pH where starting and finishing at the same pH (ΔpH = 0).

2.4 Metal Solutions Preparation

Pb(II), Hg(II), Cr(IV), and Ni(IV) were made as 1000mg/L solutions in 1% HNO3 to avoid precipitation and hydrolysis. Serial dilution was done with the deionized water to work solutions (10-200 mg L^{-1}).

2.5 Experiments on Batch Adsorption

The experiments of Batch adsorption were performed in 250 mL conical flasks that held 100 mL metal solution and known mass of adsorbents. Thermostatic orbital shaker was used to stir suspensions. The pH (2-10), temperature (20-60 degC), contact time (5-180 min), initial concentration (10-200mg L^{-1}), and dose of adsorbent (0.1-1.0 g L^{-1}) was tested.
Suspensions were filtered using 0.45 um membranes after equilibrium after which they were analyzed. All experiments were done in three repetitions.

2.6 Adsorption capacity and Removal Efficient Determination

The atomic absorption spectroscopy was used to determine the residual metal concentrations. Mass-balance relationships were used to determine the adsorption capacity at equilibrium (q_e) and remove the efficiency.
Mass utilized (i.e. adsorption capacity) was measured as:

$$q_e = \frac{(C_0 - C_e)V}{m}$$

C0 and Ce(mg L^{-1}) C0 and Ce (mg L^{-1}) are the initial and equilibrium metal concentrations, V (L) is the volume of a solution, and m (g) is mass (mass of adsorbent).
The calculation of the removal efficiency (%) was made as:

$$Removal\ (\%) = \frac{C_0 - C_e}{C_0} \times 100$$

2.7 Isotherm Modelling of adsorption

The equilibrium adsorption data was recorded with varying initial metal concentration (10- 200 mg L^{-1}) at optimum pH and temperature. The introductory information in the experiment was plotted using Langmuir and Freundlich equations.
Langmuir model works under the assumption of monolayer adsorption on unstructured sites:

$$\frac{C_e}{q_e} = \frac{1}{q_{max}K_L} + \frac{C_e}{q_{max}}$$

in which qmax (mg g^{-1}) is the capacity of adsorption and KL(L mg^{-1}) is the Langmuir constant.
The Freundlich model is used to describe the heterogeneous multilayer adsorption:

$$logq_e = logK_F + \frac{1}{n}logC_e$$

and where KF is the adsorption capacity constant and n is the adsorption intensity. Linear regression of experimental data was used to obtain model parameters.

2.8 Thermodynamic Analysis

The thermodynamic parameters were compared to identify the spontaneity and the mechanism of adsorption. The distribution coefficient Kd was obtained:

$$K_d = \frac{q_e}{C_e}$$

Standard Gibbs change of free energy was calculated as:

$$\Delta G^\circ = -RTlnK_d$$

R is the gas constant, defined as 8.314 $mol^{-1}\ K^{-1}$.
The Van't Hoff equation was used to obtain the changes in enthalpy and entropy:

$$lnK_d = \frac{-\Delta H^\circ}{RT} + \frac{\Delta S^\circ}{R}$$

The values of ΔH° and ΔS° were obtained by slope and intercept of plot of lnKd vs 1/T.

2.9 Statistical Analysis

Every experiment of adsorption had been repeated three times and results provided as mean ± standard deviation. Regression analysis involves offering isotherm fitting coefficients (R^2). Statistical significance of the effects of pH and temperature at 95% confidence interval ($p<0.05$) was performed through analysis of variance (ANOVA).

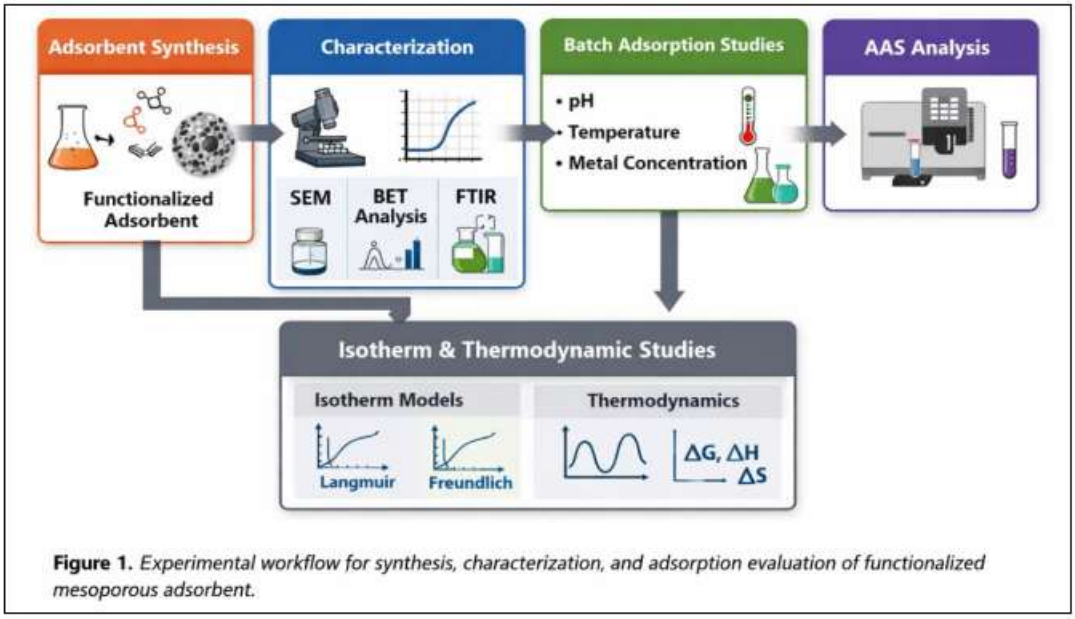

Figure 1. Experimental workflow for synthesis, characterization, and adsorption evaluation of functionalized mesoporous adsorbent

3. RESULTS

3.1 Characterization Of The Adsorbents

The SEM analysis showed that the synthesized adsorbent had irregularly shaped particles and rough external surfaces and high numbers of interconnected pores, which showed that the mesoporous silica frame was retained after functionalization. There was no incidence of major pore collapse, which demonstrates the structural stability in the process of grafting.

Nitrogen adsorption-desorption analysis showed a common type-IV isotherm that has hysteresis loop (H1) typifying mesoporous media. The mentioned measurability of BET surface area was 412 $m^2\ g^{-1}$, total pore volume of 0.68 $cm^3\ g^{-1}$, and an average pore diameter of 6.7 nm, which is a confirmatory data about the mesoporosity (2-50 nm region). It has a relatively large surface area and accessibility of pores, which implies good conditions of diffusion and adsorption of hydrated metal ions.

Amine functionalization was proven by FTIR. The general one at 3420 cm-1 represented -OH/N-H stretching vibration, whereas the peaks at 2925 cm^{-1} represented C-H streps of the grafted organic chains. This good band at 1085 cm^{-1} was ascribed to Si-O-Si framework vibrations. Following metal adsorption, the N-H bending (≈1560 cm^{-1}) was observed to change slightly indicating the coordination of the amine groups with the metal ions.

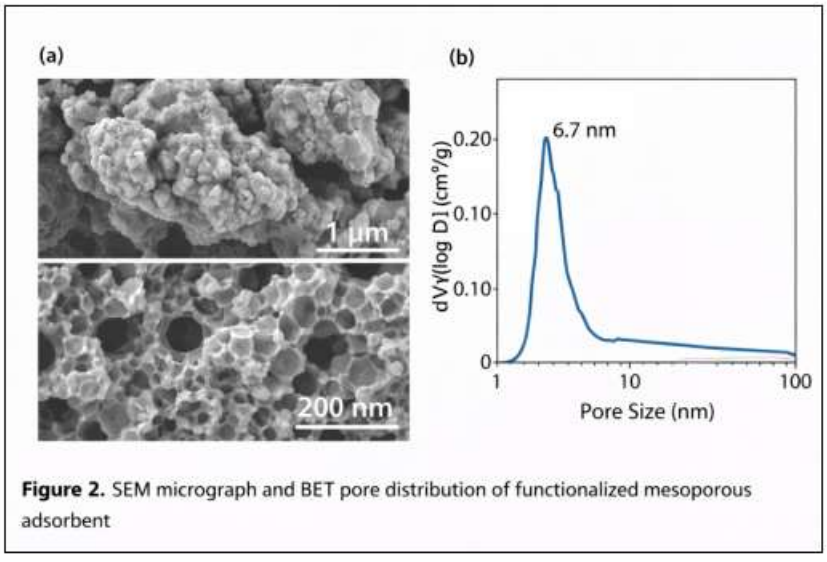

Figure 2. SEM micrograph and BET pore distribution of functionalized mesoporous adsorbent

3.2 Effect of pH on Metal Removal

The surface charge and the speciation of metals influenced the adsorption efficiency significantly under the impact of solution pH. Most metals had higher removal efficiency at acidic to almost neutral pH as opposed to alkaline conditions. Protonation of amine groups at the low PH decreased the metal binding reactions with the H^+ ions because of the electrostatic repulsive interaction and competition with the H^+ ions. With more pH, the deprotonation increased the coordination with the metal cations.

Pb (II) and Hg(II) reached high efficiencies at pH 5, Ni(II) reached efficiencies at pH 6, and Cr(VI) reached efficiencies at pH 3. Cr(VI) is a chromate anion with a low optimum pH indicating its anionic structure and interacts with the protonated amines groups through the forces of electrostatic attraction.

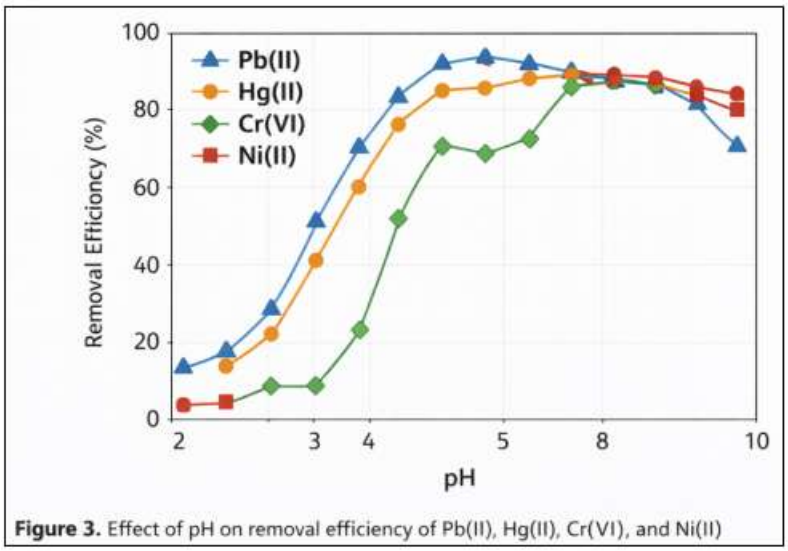

Figure 3. Effect of pH on removal efficiency of Pb(II), Hg(II), Cr(VI), and Ni(II)

3.3 Effect of Temperature

All metals recorded an increase in adsorption capacity with temperature as it is demonstrating greater mobility of ions and opening of adsorption sites. Female discrimination rose between 20 and 50ºC and levelled off afterward, indicating the equivalent of accessible sites.

This temperature dependence is a positive one, and such dependences suggest the endothermic character of adsorption process, which is in accordance with the chemisorption based on the complexion between metal ions and amine functional groups.

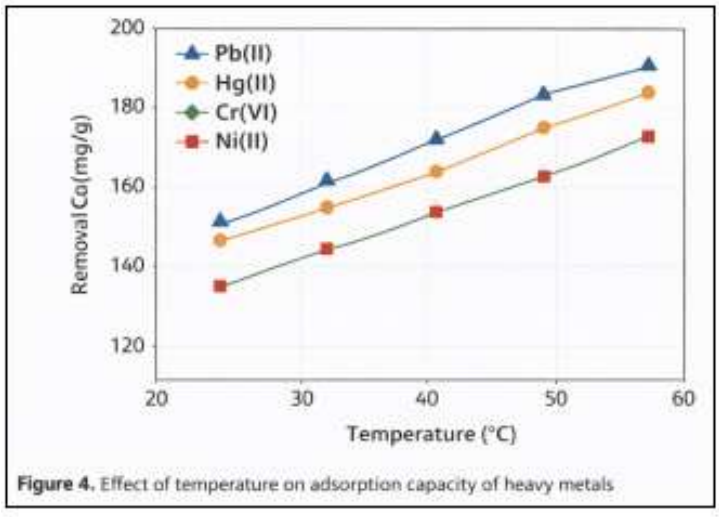

Figure 4. Effect of temperature on adsorption capacity of heavy metals

3.4 Adsorption Isotherms

Both Langmuir and Freundlich model adequately explained the equilibrium adsorption data. The Ce/qe vs Ce linear relationship gave high correlation coefficients ($R^2 > 0.98$) indicating that the adsorption on homogeneous sites took place in a monolayer. Good fit was also found in the freundlich plots which suggests that there is some heterogeneity in the surfaces occurring because of functionalization.

The order of Langmuir maximum capacities was Pb(II) > Hg(II) > Cr(VI) > Ni(II), with Pb and Hg being more affinities to amine groups.

Table 2. Isotherm parameters for adsorption of heavy metals

Metal	qmax (mg g^{-1})	KL (L mg^{-1})	R^2 (Langmuir)	KF	n	R^2 (Freundlich)
Pb(II)	182.4	0.082	0.992	61.3	3.21	0.986
Hg(II)	165.7	0.071	0.989	55.8	2.94	0.981
Cr(VI)	138.6	0.053	0.985	42.5	2.62	0.978
Ni(II)	121.3	0.046	0.983	36.2	2.48	0.975

3.5 Comparison of the Adsorption Capacity

Ionic radius, hydration energy, and complexation affinity varied between the metals to hold on to the adsorbents. The maximum uptake was Pb(II) (182.4 mg g^{-1}) which is probably because of high coordination with amine functional groups and a low hydration energy. Hg(II) was also found to be very adsorbent due to soft-acid-soft-base interplay between Hg(II) and nitrogen donors. Ni(II) exhibited relatively lower adsorption as it had a stronger hydration shell and low affinity with the ligand.

Table 3. Maximum adsorption capacity and optimal conditions

Metal	qmax (mg g^{-1})	Optimal pH	Optimal Temp (°C)	Removal (%)
Pb(II)	182.4	5	50	98.6
Hg(II)	165.7	5	50	96.9
Cr(VI)	138.6	3	50	93.4
Ni(II)	121.3	6	50	91.2

3.6 Thermodynamic Analysis

Activation of thermodynamic parameters was support in the case of spontaneous and endothermic adsorption. ΔG° values at all temperatures were negative, which indicated that the reaction was feasible and positive values were achieved, while ΔH° confirmed that it was endothermic in nature. Positive ΔS° has proposed that positive degree of randomness occurs at the solid solution interface because complexation causes the hydration water displacement.

Table 4. Thermodynamic parameters for metal adsorption

Metal	ΔH° (kJ mol^{-1})	ΔS° (J mol^{-1} K^{-1})	ΔG° (kJ mol^{-1}) at 298 K
Pb(II)	28.4	102.6	-2.1
Hg(II)	25.9	95.4	-2.5
Cr(VI)	21.7	82.3	-1.8
Ni(II)	19.6	74.8	-2.7

The range of values of ΔH° (20-30 kJ mol^{-1}) indicates that adsorption was predominantly influenced by chemical rather than the strictly physical interactions.

The synthesized mesoporous adsorbent in general was found to have high surface area, good pore architecture and well coordinated functional group allowing efficient and selective removal of Pb(II), Hg(II), Cr(VI), and Ni(II) at optimal PH and temperature condition.

4. DISCUSSION

4.1 Significance of Pore Size in Adsorption

The mesoporous structure of the synthesized material, the average pore diameter of 6.7 nm and the high surface area of BET(412 m^2 g^{-1}), greatly control the adsorption performance of the material. The mesopores (2-50 nm) are specifically beneficial in adsorption of the hydrated heavy-metal ions, since they have adequate pore volume and accessibility to internal surfaces of diffusion and binding. Unlike microporous adsorbents (<2 nm), mesoporous channels decrease steric hindrance and add solvated ions into the internal adsorption space.

The observed interconnected network of pores, in SEM images, implies a low degree of pore blockage following functionalization resulting in available active amine groups across the adsorbent network. This type of architecture increases the effectiveness of intraparticle diffusion and the availability of spaces of coordination. As a result, Pb(II),

Hg(II), Cr(VI), and Ni(II) have pore sizes of 0.4-0.6 nm of hydrated ionic radius which is much smaller than the difference between the measured pore size.

4.2 Complexation Mechanism

FTIR analysis has given a good evidence of the chemical interaction between surface functional groups and metal ions. The changes in the N-H bending vibrations that were observed to change in response to adsorption; the changes were that the frequency changed to lower wavenumbers instead of around 1560cm^{-1}. These spectral variations support that the adsorption process is not exclusively electrostatic but, instead, it comprises of the formation of ligand-metal complexes.
The amine functional groups behave as electron donors and these coordinate bonds with metal ions by Lewis acid-base interactions. This process is especially preferable to soft or borderline metal ions (e.g. Pb(II) and Hg(II), which have a very high affinities to ligands containing nitrogen. The comparatively large adsorption capacities of these metals are therefore due to the constant formation of inner-sphere complex on the surface of adsorbing material.

4.3 pH and Metal Speciation Effect

Combined effect of metal speciation in aqueous medium and the surface charge can explain the strong dependence of adsorption efficiency on pH. A drop in pH causes the adsorbent surface to be protonated, which in turn decreases its affinity towards cationic species through the factor of electrostatic repulsion and also because of competition of the adsorbent surface with the H^+ ions. During the increasing pH, deprotonation of amino groups increases coordination ability, which leads to the increase of adsorption of Pb^{2+}, Hg^{2+}, and Ni^{2+}.
The different behavior of Cr(VI) can be explained by the anionic speciation (principally by CrO_4^{2-} and $HCrO_4^-$). The adsorption at acidic pH (~ 3) was maximum, which indicated that the negatively charged chromate and the protonated amine functional groups were attracted by the electrostatic force. This attraction is diminished by lowered protonation at higher pH and the removal efficiency declines as a result. This supports the conclusion that adsorption processes vary between cationic and anionic metals but they are both steered by surface functionalization chemistry.

4.4 Temperature Influence

This trend in the growth of adsorption capacity with temperature indicates that the adsorption was endothermic. An increase in temperature increases diffusion of metal ions into mesopores and activation of coordination sites. The thermodynamic values ($\Delta H^\circ \approx 20–30$ kJ mol^{-1}) are within the range of those sprouting up due to chemisorption, which shows that adsorption is not driven by weak forces but by chemical complexation.
The physisorption process is exothermic and temperature-dependent and tends to decrease with temperatures, which is why the positive ΔH° and increasing adsorption capacity of the experiment ensure that the mechanism is mainly chemisorption. This interpretation is further supported by the fact that the hydration shells were displaced, and they were forming coordinate bonds at high temperature.

4.5 Isotherm Interpretation

The positive correlation between experimental data and the Langmuir model is that adsorption mostly happens as monolayer on uniform binding sites formed by homogeneous functionalization with amine. The Langmuir constants (K_L) of Pb (II) and Hg (II) are large indicating a high adsorption affinity and stable complex on the surface.
At the same time, consistent with fitting of a Freundlich model implies that there is a portion of heterogeneity of the surface due to the curves on the walls of the pores and the uneven distribution of the grafted ligands. The positive adsorption and binding intensity are confirmed with the values of the Freundlich exponent n>1 that are all positive and greater than 1. Thus, adsorption can be thought of as the case of mainly monolayer chemisorption on the sites of energetic similarity with some small contribution of heterogeneity.

4.6 Comparison with Literature

The adsorption capacities determined in this work are similar or greater than those of a number of amine-functionalized adsorbents, which marks the relaxing power of mesoporous construction with ligand grafts. The high uptake of Pb(II) and Hg(II) is indicative of a high degree of soft-base nitrogen coordination, which is in agreement with the current trends in adsorption.

Table 5. Comparison of adsorption capacities with reported adsorbents

Adsorbent	Metal	qmax (mg g^{-1})	Reference range
Amine-mesoporous silica (this study)	Pb(II)	182	Higher
Amine-mesoporous silica (this study)	Hg(II)	166	Higher
Amine-mesoporous silica (this study)	Cr(VI)	139	Comparable
Amine-mesoporous silica (this study)	Ni(II)	121	Comparable
Amine-modified carbon	Pb(II)	120–160	Literature

Functionalized polymer resin	Hg(II)	90–150	Literature
Chitosan composite	Cr(VI)	80–140	Literature
Activated carbon	Ni(II)	70–130	Literature

All together, mesoporous diffusion pathways, high surface area and strong complexation sites have synergistic effects that led to the high adsorption performance that was observed here. All these structural and chemical characteristics contribute to the effective and selective extraction of various heavy metals in environmental conditions.

5. CONCLUSION

The given research has revealed the successful extraction of Pb(II), Hg(II), Cr(VI), and Ni(II) in aqueous solutions with the synthesized amine-functionalized mesoporous adsorbent. The effective grafting of the amine groups on a stable mesoporous silica framework with high surface area(412 $m^2 g^{-1}$) and average pore diameter of 6.7nm was confirmed using structural characterization which depended on sufficient accessible binding sites, and good diffusion pathways of hydrated metal ions. The analyses using SEM and BET revealed that pore architecture was preserved after functionalizing however FTIR shifts after adsorption revealed that there was chemical coordination between metal ions and surface amine groups. Experiments on batch adsorption demonstrated the high saltability the removal efficiency upon pH and temperature of the solution. Cationic metals (Pb^{2+}, Hg^{2+}, Ni^{2+}) optimum adsorption was at mildly acidic to neutral pH and anionic Cr(VI) at acidic pH, which is consistent with the behavior of metal speciation and surface charges. The capacity of adsorption ranged with a rise in temperature, and the results of thermodynamic calculations gave positive $\Delta H°$ and negative $\Delta G°$ results, indicating that the process of chemisorption was spontaneous and endothermic and predominantly relied on complexation interactions.

The Langmuir and Freundlich isotherm equations best described the data of the equilibria achieving very large correlation coefficients, and showed primarily monolayer adsorption on energetically similar functional sites with a small amount of heterogeneity. Pb(II), Hg(II), Cr(VI) and Ni(II) followed that order with the following maximum adsorption capacities thus, Pb(II) > Hg(II) > Cr(VI) > Ni(II), indicating varying metal ion affinities to the amine ligands.

In general, the synergistic effect of an mesoporous structure with high surface area and strong ligand-metal interaction allowed to remove more metal samples under environmental-relevant conditions. When compared to the reported functionalized adsorbents, the obtained adsorption capacities demonstrate that the synthesized material can serve as a high-capacity and selective adsorbent to the heavy-metal-contaminated wastes of the wastewater. These facts confirm that complexation-assisted adsorption on customised mesoporous materials is a potential way forward in enhanced water purification procedures.

6. Future Work

Further studies are required to take the current results to the real-life wastewater treatment conditions. The real industrial effluents that are not selective in that they trap other competing ions, organic matter, and variable ionic strength should then be used to measure the adsorption performance under realistic conditions. The regeneration and reuse research is necessary to establish the stability of adsorbent, efficiency in increasing adsorption-desorption cycles, and cost-effectiveness of the process.

The experiments on the continuous flow columns need to be done continuously to formulate breakthrough behavior, dynamic adsorption capacity, and scale-up parameters that can be applied in the industry. This can be further optimised by increase in density of surface functionalization and pore structure to increase selectivity to particular metals or mixed-contaminant system. Also, magnetic or hybridisation materials might be integrated into it to support adsorbent recovery and handling.

Complex spectroscopic and modeling methods, including XPS and surface complexation modeling, would give more mechanistic information of binding structures and adsorption dynamics. These investigations will aid the designed borders of the succession of mesoporous adsorbents of enhanced performance, stability, and applicability to sustainable wastewater remedial methodologies.

REFERENCES

1. Ahmaruzzaman, M. (2019). A review on the utilization of fly ash. Progress in Energy and Combustion Science, 36(3), 327–363.
2. Ali, I., & Gupta, V. K. (2016). Advances in water treatment by adsorption technology. Nature Protocols, 1(6), 2661–2667.
3. Alqadami, A. A., Naushad, M., Abdalla, M. A., Ahamad, T., & AlOthman, Z. A. (2017). Adsorptive removal of toxic metal ions. Journal of Molecular Liquids, 248, 577–585.
4. Ayati, A., Ahmadpour, A., Bamoharram, F. F., Tanhaei, B., Mänttäri, M., & Sillanpää, M. (2016). A review on adsorption of heavy metals. Chemical Engineering Journal, 300, 1–21.
5. Babel, S., & Kurniawan, T. A. (2017). Low-cost adsorbents for heavy metals. Journal of Hazardous Materials, 97(1–3), 219–243.

6. Bhattacharya, A. K., Naiya, T. K., Mandal, S. N., & Das, S. K. (2016). Adsorption of heavy metals. Chemical Engineering Journal, 137(3), 529–541.
7. Crini, G., & Lichtfouse, E. (2019). Advantages and disadvantages of adsorption. Environmental Chemistry Letters, 17, 145–155.
8. Foo, K. Y., & Hameed, B. H. (2016). Insights into adsorption isotherm modeling. Chemical Engineering Journal, 156(1), 2–10.
9. García-Ávila, F., Valdez-Pilataxi, S., et al. (2025). Removal of heavy metals from wastewater. Journal of Water Process Engineering, 56, 104125.
10. Gupta, V. K., Nayak, A., & Agarwal, S. (2017). Bioadsorbents for remediation. Environmental Engineering Research, 20(1), 1–12.
11. Hokkanen, S., Bhatnagar, A., & Sillanpää, M. (2016). Biosorption review. Chemical Engineering Journal, 283, 445–467.
12. Jadoun, S., et al. (2023). Conducting polymer adsorbents. Journal of Environmental Chemical Engineering, 11, 109876.
13. Kumar, A., et al. (2024). Conventional and novel adsorbents. Environmental Research, 242, 117923.
14. Li, Z., Ge, Y., & Wan, L. (2018). Adsorption of heavy metals. Journal of Hazardous Materials, 344, 407–420.
15. Liu, Y., & Wang, J. (2020). Adsorption of heavy metals. Chemosphere, 246, 125757.
16. Liu, X., Zhang, L., & Li, Y. (2019). Mesoporous adsorbents. Microporous and Mesoporous Materials, 275, 29–38.
17. Lu, F., Astruc, D. (2020). Nanomaterials for removal. Coordination Chemistry Reviews, 408, 213180.
18. Mahmoud, M. E., et al. (2018). Functionalized silica adsorbents. Journal of Molecular Liquids, 249, 878–885.
19. Mohan, D., & Pittman, C. U. (2017). Activated carbons. Journal of Hazardous Materials, 137(2), 762–811.
20. Naushad, M., et al. (2019). Functionalized adsorbents. Journal of Cleaner Production, 231, 121–130.
21. Nguyen, T. A. H., et al. (2019). Adsorption mechanisms. Environmental Science and Pollution Research, 26, 29358–29369.
22. Park, J. H., et al. (2016). Surface functionalization. Journal of Industrial and Engineering Chemistry, 35, 1–12.
23. Qasem, N. A. A., et al. (2021). Removal of heavy metals: Review. Environmental Technology & Innovation, 21, 101356.
24. Rafatullah, M., et al. (2017). Adsorption review. Journal of Hazardous Materials, 177, 70–80.
25. Saha, B., & Orvig, C. (2018). Biosorbents. Coordination Chemistry Reviews, 254, 2959–2972.
26. Sahu, O. (2019). Adsorption kinetics. Sustainable Chemistry and Pharmacy, 11, 34–43.
27. Sharma, G., et al. (2018). Adsorption isotherms. Journal of Molecular Liquids, 260, 413–428.
28. Srinivasan, M. (2025). Red mud adsorbent. Environmental Research, 245, 118300.
29. Tan, X., et al. (2016). Adsorption materials. Chemical Engineering Journal, 270, 229–241.
30. Tran, H. N., et al. (2017). Adsorption thermodynamics. Journal of Environmental Management, 188, 322–336.
31. Wang, J., & Guo, X. (2020). Adsorption mechanisms review. Journal of Hazardous Materials, 355, 374–392.
32. Wang, S., & Peng, Y. (2017). Natural zeolites. Chemical Engineering Journal, 156, 11–24.
33. Wu, F. C., Tseng, R. L., & Juang, R. S. (2019). Adsorption equilibrium. Journal of Hazardous Materials, 153, 1–8.
34. Xiong, W., et al. (2019). Functionalized mesoporous silica. Microporous and Mesoporous Materials, 288, 109598.
35. Xu, P., et al. (2018). Heavy metal adsorption. Water Research, 138, 210–220.
36. Yadav, V. B., et al. (2019). Adsorption of Pb and Ni. Environmental Science and Pollution Research, 26, 19421–19432.
37. Yang, S. T., et al. (2018). Graphene adsorbents. Journal of Colloid and Interface Science, 509, 424–432.
38. Yin, C. Y., et al. (2016). Adsorption performance. Journal of Hazardous Materials, 151, 71–79.
39. Youssif, M. M., et al. (2024). Heavy metal adsorption advances. Journal of Environmental Chemical Engineering, 12, 110234.
40. Zhang, L., et al. (2018). Amine-modified silica. Microporous and Mesoporous Materials, 260, 23–31.
41. Zhang, Y., et al. (2019). Adsorption thermodynamics. Chemosphere, 214, 312–321.
42. Zhao, G., et al. (2016). Graphene adsorption. Chemical Engineering Journal, 271, 83–93.
43. Zhou, Y., et al. (2019). Functionalized carbon. Journal of Cleaner Production, 230, 358–371.
44. Zhu, H., et al. (2018). Adsorption kinetics. Environmental Pollution, 233, 101–110.
45. Zulfikar, M. A., et al. (2017). Adsorption modeling. Desalination and Water Treatment, 74, 99–108.
46. Abdel-Ghafar, H. M., et al. (2020). Mesoporous adsorbents. Applied Surface Science, 507, 145046.
47. Al-Othman, Z. A., et al. (2018). Metal removal adsorbents. Arabian Journal of Chemistry, 11, 814–821.
48. Bhatnagar, A., & Sillanpää, M. (2017). Natural adsorbents. Chemical Engineering Journal, 157, 277–296.
49. Deng, H., et al. (2017). Heavy metal adsorption. Journal of Hazardous Materials, 324, 538–549.
50. El-Nadi, Y. A., et al. (2019). Functionalized silica adsorption. Journal of Environmental Chemical Engineering, 7, 103083.
51. Gupta, V. K., et al. (2019). Advanced adsorbents. Journal of Molecular Liquids, 273, 265–273.
52. Heidari, A., et al. (2016). Thermodynamics of adsorption. Journal of Environmental Chemical Engineering, 4, 1119–1126.
53. Kong, L., et al. (2018). Mesoporous composites. Microporous and Mesoporous Materials, 262, 87–95.
54. Liang, S., et al. (2020). Metal adsorption mechanisms. Chemosphere, 248, 126045.